Results in Physics 76 (2025) 108398

Contents lists available at ScienceDirect

Results in Physics

journal homepage: www.elsevier.com/locate/rinp

Intensity correlations in scattered vector vortex beams for determining the topological charge

Patnala Vanitha, Do-Kyeong Ko *

Department of Physics and Photon Science, Gwangju Institute of Science and Technology, Gwangju 61005, Republic of Korea

ARTICLE INFO

Keywords:
Vector vortex beams
Auto-correlation function
Scattering
Speckles
Topological charge

ABSTRACT

We propose a novel scheme for measuring the topological charge (TC) of the vector vortex beam (VVB) using polarization speckles size of the 2D auto-correlation function of scattered vector vortices. We have generated the non-separable state having singularities in both orbital angular momentum (OAM) and polarization. This non-separability is verified by measuring the degree of polarization (DOP) which can be calculated by using Stokes parameters. The Stokes parameters can be measured by observing the intensity distribution of the beam when projected onto different polarization states. The divergence of polarization speckle size of the auto-correlation function was measured as a function of topological charge of the vector vortex beams. These results can be used to generate a security key for data authentication and data encryption.

Introduction

A system is called entangled, when its state cannot be expressed as the product of two individual states [1]. Generally, one uses the entanglement between two spatially separated particles in the same degree of freedom (DOF) such as spin or polarization. In some cases, hybrid entanglement occurs when two degrees of freedom of either a single particle or two particles are entangled [2,3]. This arises due to the non-separability of two degrees of freedom. Similar kind of non-separability can also be seen in classical optics, when we consider the radially polarized light beams [4]. The entanglement that can be used to describe the non-separability of classical light named as the “classical entanglement”. These non-separable states of light are shown to violate Bell like inequality [5]. The non-separability of vector beams is utilized in many applications such as free space optical communication, high speed kinematic sensing, polarization metrology, single shot Mueller polarimetry, and characterizing the quantum channels [6–10]. The violation of Bell’s inequality by non-separable vector beams reveals entanglement-like correlations between spatial and polarization degrees of freedom, correlations that cannot be explained by classical local theories. This highlights their potential for advancing communication, sensing, and information processing technologies, while also offering insights into the boundary between classical and quantum regimes.

The phase singular beams, also known as vortex beams, possess zero intensity at the beam’s center and carry an orbital angular momentum (OAM) of $\pm l\hbar$ per photon, where l is the topological charge (TC) of vortex beam, which can be defined as the number of helices per wavelength [11]. In another case, one can use this OAM as an additional degree of freedom along with the polarization to form the hybrid entanglement state [2]. The vector beams are known for their non-separability in the spatial mode and polarization DOFs. Such non-separability is essential for advanced optical technologies because it enables multiplexing and improves control over light’s spatial and polarization properties, benefiting applications such as high-capacity optical communication, polarization metrology, quantum simulation, imaging, and information processing. The non-separable beams can be generated using interferometers, resonators, spatial light modulators (SLMs), digital micromirror devices (DMDs), or q-plates [12–16].

In the past, the scattering of vector vortex beams has been thoroughly studied [17–19]. A coherent light beam can be scattered to produce fine granular patterns of light known as the speckle patterns. These speckle patterns are formed due to the interference of many scattered wave fronts coming from different inhomogeneities of a rough surface on the detection plane [20]. The speckles and their statistical properties are utilized in various applications such as optical imaging, optical coherence tomography, and astronomy [21–23]. Past studies on the scattering of optical vortices have revealed that the intensity speckle size decreases with the vortex order, which is attributed to the larger area of illumination on the rough surface [24]. A more detailed theoretical understanding of this behavior is provided by J. W. Goodman

* Corresponding author.
E-mail address: dkko@gist.ac.kr (D.-K. Ko).

https://doi.org/10.1016/j.rinp.2025.108398
Received 13 March 2025; Received in revised form 29 July 2025; Accepted 16 August 2025
Available online 18 August 2025

[25]. In contrast, speckle fields with spatially varying polarization referred to as polarization speckles have attracted significant interest in biomedical optics, particularly for their potential in differentiating between various types of skin cancer [26]. Further insights into the formation, behavior, and diagnostic potential of polarization speckles in biological tissues are discussed in studies by Shirai and Dogariu (2016) and Alfano (2010), which provide comprehensive physical interpretations and applications [27,28]. These polarization speckles can be generated by the superposition of two speckle patterns obtained from orthogonally polarized beams scattered through statistically independent random media [19]. The physical origin of these polarization speckles lies in spatial fluctuations of the orthogonal polarization components induced by scattering, a mechanism that is clearly and comprehensively explained [19]. The size of the polarization speckles decreases with the order of the vortex, and also changes slightly with different polarization states.

For the utilization of vector vortex beams in communication where one can enhance the data capacity by four times, we need to propagate them through the channel. After propagating through the channel, the mode and polarization information gets disturbed and one needs to recover both the mode and polarization information. For compensating the polarization changes, an approach involving Mueller matrix and SU (2) operations using wave plates was developed [29]. There are many techniques to measure the topological charge of the vector vortex beams, but they are not suitable for partially coherent or incoherent vortices [30–32]. A limited number of techniques are available for finding the topological charge of the partially coherent vector vortex beam [33–37].

In this work, we generate light beams with non-separable OAM and polarization and confirm the non-separability using the degree of polarization [38]. A polarizing Sagnac interferometer is used to generate the non-separable beams by placing a dove prism along with a spiral phase plate (SPP). The generated non-separable beam is projected onto different polarizations using a quarter-wave plate (QWP) and a polarizer, and the corresponding intensity distribution is measured. The degree of polarization is zero for the maximally non-separable state i.e., the non-separable state is completely unpolarized. One can use the 2D spatial auto-correlation technique to find the information about topological charge of the scattered vector vortex beams. Here, the topological charge of the vector vortex beam refers to the topological charge with either integers or fractional values. In section 2, we present the theoretical details of the intensity distributions of non-separable state which is projected onto different polarization states and also the proof of this non-separability using degree of polarization. In section 3, we present an experimental setup to generate the polarized states and investigate their scattering through the ground glass plate (GGP). The results along with their detailed interpretation are presented in section 4 and followed by the conclusions in section 5.

Theoretical analysis

A classical light beam with a non-separable state of OAM and polarization can be represented mathematically as [38]:

$$|\psi\rangle = |H, +l\rangle + |V, -l\rangle, \tag{1}$$

where $|H\rangle$, $|V\rangle$ and $|+l\rangle$, $|-l\rangle$ are the basis vectors of vector spaces corresponding to the polarization and OAM, which are independent. The density matrix of the state of polarization, represented by a Poincare sphere, can be completely described by:

$$\rho_p = \frac{1}{2}\sum_{i=1}^{3}\sigma_i * s_i, \tag{2}$$

where, $\sigma_i' s$ are the Pauli matrices, $s_i' s$ are the Stokes parameters of the corresponding polarization state and '*' indicates the multiplication between the two operators. The trace of this density matrix is given by:

$$Tr\left[\rho_p^2\right] = \frac{1}{2}\left(1 + s_1^2 + s_2^2 + s_3^2\right) = \frac{1}{2}\left(1 + \mathrm{DOP}^2\right), \tag{3}$$

where DOP denotes the degree of polarization which can be measured using the magnitude of the Stokes vectors $\sqrt{s_1^2 + s_2^2 + s_3^2}$. If the DOP is zero, the generated state is purely non-separable and completely unpolarized. Experimentally, one can easily find the DOP by measuring the Stokes parameters using the power meter. For a separable state, the outcome of one does not affect the outcome of the other, whereas, in case of a non-separable state, the outcome in one depends on the other outcome due to the fact that the OAM state of the beam varies according to the projections to different polarization states. The general expression for the polarization state is given as:

$$|\zeta\rangle = \cos(\theta)|H\rangle + \exp(i\phi)\sin(\theta)|V\rangle, \tag{4}$$

where, θ and ϕ are the Euler angles corresponding to the polarization state on the Poincare sphere. Using Eqs. (1) and (4), we obtain the superposition of the OAM state as:

$$|\psi_{OAM}\rangle = \langle\zeta|\psi\rangle = \cos(\theta)|l\rangle + \exp(-i\phi)\sin(\theta)|-l\rangle. \tag{5}$$

The above equation represents a pure OAM superposition state. The transverse intensity profile of the beam corresponds to the superposition of two equal and oppositely charged vortices with different polarization states. Therefore, the intensity profile of the beam varies according to the polarization projections defined by θ and ϕ. For demonstration, we consider $(\theta,\phi) = (0,0), (90,0), (45,0), (-45,0), (45,90), (-45,90)$ which correspond to $|H\rangle$, $|V\rangle$, $|D\rangle = |H\rangle + |V\rangle$, $|AD\rangle = |H\rangle - |V\rangle$, $|RCR\rangle = |H\rangle + i|V\rangle$, and $|LCR\rangle = |H\rangle - i|V\rangle$ polarization states, respectively.

Experimental details

The experimental setup for generating the vector vortices (non-separable state) is shown in Fig. 1. An incident He–Ne laser beam of wavelength 633nm and power 5mW is used to generate vector vortex beams. Here, the incident laser beam is confined along the horizontal polarization which is parallel to the optical plane using the half-wave plate (HWP). The Sagnac interferometer has the advantage that the interfering beams follow exactly the same path, making the output insensitive to phase fluctuations. This method is used for the decomposition of topological charge-l polarization vortex beam into the coherent sum of two-phase vortex beams with opposite sign of topological charges of $\pm l$ and opposite handedness of polarizations. Then this input beam passes through the polarizing Sagnac interferometer containing a Dove prism (used to change the sign of the topological charge along one beam path), spatial light modulator and half-wave plate (used to change the direction of polarization) to generate two light beams with different topological charge and polarization states. These two light beams with different topological charge and polarizations are superposed onto the beam splitter to generate the non-separable state. A computer-generated hologram (CGH) can be created by the interference of a vortex beam with the Gaussian beam, and it is displayed on the spatial light modulator (Holoeye PLUTO-2.1-NIR-144) which is used to generate vortex beams. In our experiment, the SLM is used at small incidence angle to minimize astigmatism caused by the quadratically varying optical thickness of the SLM.

The intensity distributions corresponding to the different polarizations are recorded using a CCD camera (UI-2220SE-M) with a resolution of 768 × 576 pixels and a pixel size of 8.3 μm. The Stokes parameters can be obtained by changing the angles in quarter-wave plate (θ) and polarizer (ϕ), which were explained in the previous section 2. We project non-separable beam to horizontal(H), vertical(V), diagonal (D), anti-diagonal (AD), right circular (RCR) and left circular (LCR) polarizations and measure the intensity. The intensity measurements for

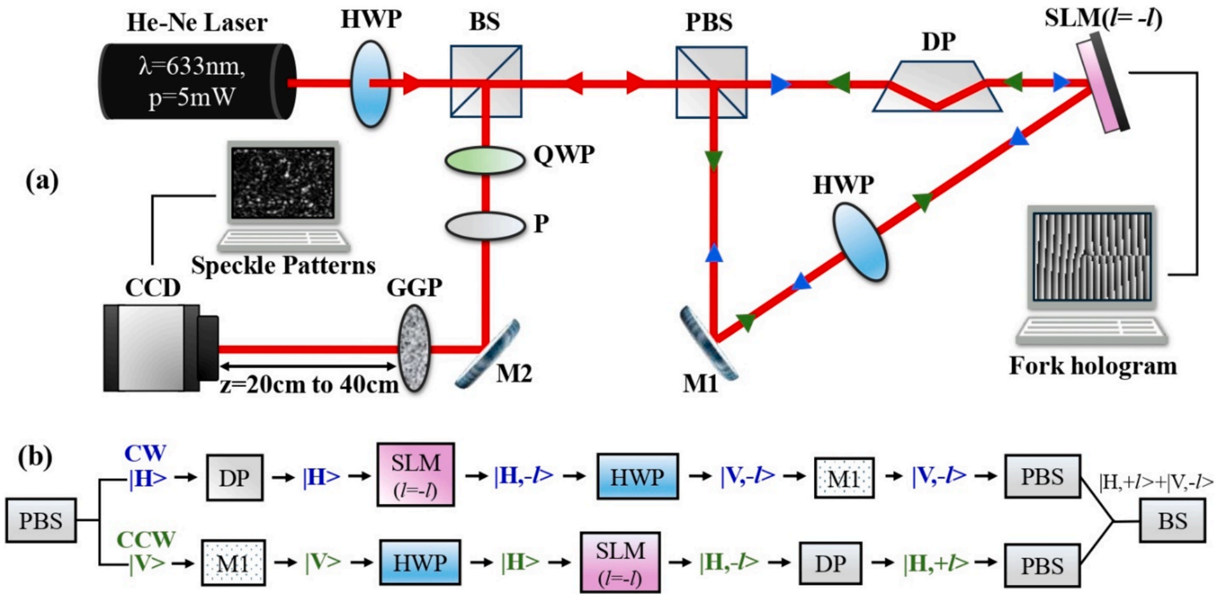

Fig. 1. (a) Experimental setup for the generation of vector vortices and their corresponding speckle patterns, (b) Optical beam passage inside the Sagnac interferometer.
HWP – half-wave plate, BS – beam splitter, PBS – polarized beam splitter, DP – dove prism, SLM – spatial light modulator, M1 & M2 – mirrors, QWP – quarter-wave plate, P – polarizer, GGP – ground glass plate, CCD – charge coupled device, CW – clockwise, CCW – counter clockwise.

determining the Stokes parameters $s_1 = (I_H - I_V)/I$, $s_2 = (I_D - I_{AD})/I$, and $s_3 = (I_{RCR} - I_{LCR})/I$ were performed with an optical power meter (Thorlabs PM100D) with sensitivity of 1nW, where I is the total intensity of the light beam and I_X is the intensity of the beam corresponding to the x polarization. The obtained polarization states are scattered through a GGP ground glass plate (Thorlabs DG10-600) to generate random patterns [19] and are recorded using a CCD camera as shown in Fig. 1(a). Fig. 1(b) shows the optical beam passage inside the Sagnac interferometer.

Results and discussion

We start the experiment by recording the intensity distributions of coherent light beam with non-separable state which is projected onto the different polarizations for the vector vortex beams at the plane of GGP for a range of all the topological charges starting from 1 to 5 with an interval of 0.5. Fig. 2 shows the experimental (first and third rows) and the theoretical (second and fourth rows) intensity distributions corresponding to the different projections of the polarization states for an order $l = 1$ and 1.5. The experimental results are consistent with the theoretical results. When we project the non-separable state on

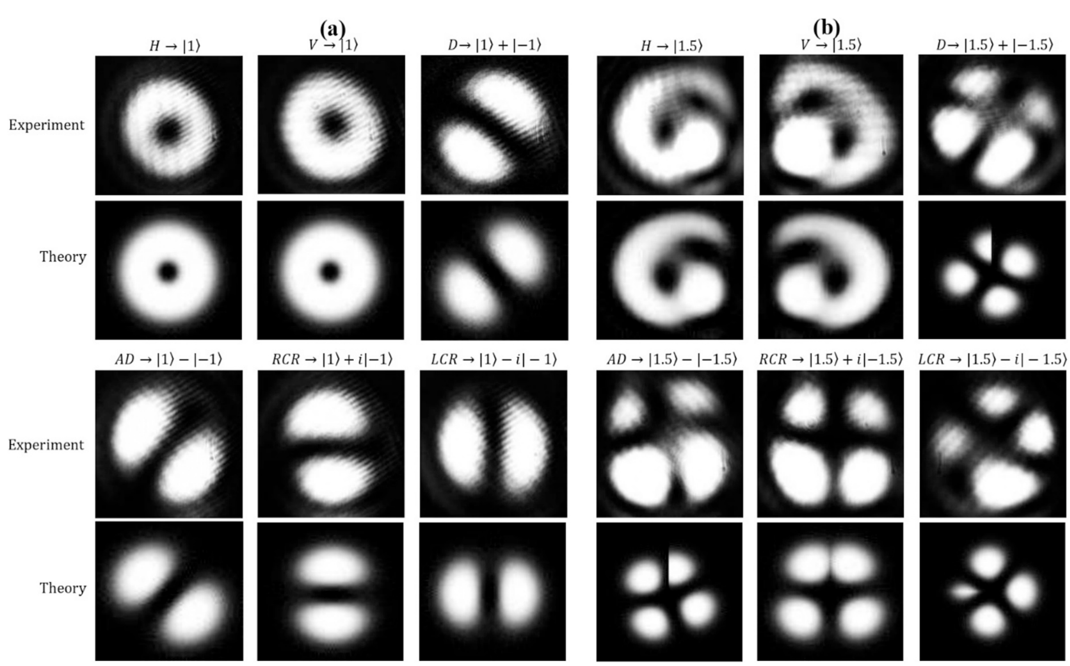

Fig. 2. Experimental and theoretical intensity distributions of the non-separable states of light beam with (a) $l = 1$, (b) $l = 1.5$ for different polarization projections and OAM states corresponding to each intensity distribution are also given.

horizontal (vertical) polarization, we obtain vortex order $l = +1$ (-1). The projections of the non-separable state on diagonal (D), anti-diagonal (AD), left circular (LCR) and right circular (RCR) gives the superposition of two orthogonal vortices that contain $2l$ number of lobes with different orientations. The number of lobes confirms the order or the topological charge of the vortex and the change in the orientation of lobes confirms the presence of non-separability in a light beam. We measure both the Stokes parameters of the coherent light beam for non-separable state and the degree of polarization of the beams before the GGP and the results s_i = -0.04, −0.07, 0.06 and DOP = 0.01 have been shown. One can clearly see that the non-separable state is completely unpolarized. The deviations in the degree of polarization may be due to uncertainties associated with the orientation of the waveplates, small misalignment of the interferometer and the measurement uncertainty of the power meter.

After measuring the intensity distributions of the non-separable beam, we scattered them through the GGP and recorded the speckle patterns corresponding to different orders of the vector vortex beams by placing a camera immediately after the GGP. Fig. 3 shows the speckle patterns obtained by scattering the vector vortex beams at different orders $l = 1$–3 with an interval of 0.5 (from left to right) at a particular propagation distances z = 20 cm. The color maps and length scales have also been shown in the same figure. It is clear from the figure that the size of the speckle decreases with an increase in the order of the vector vortex beams which is attributed to the increase in the area of illumination on the rough surface with the order. One can use the speckle patterns to generate a security key in 1D cryptography systems.

Theoretically, the reduction in polarization speckle size with increasing TCs can be understood in the following way: the helical phase structure of the vortex beam becomes more intricate upon increasing the TC of the beam. This, in turn, introduces higher spatial frequency components which leads to finer variations in intensity and polarization distributions across the beam profile. Since the speckle size is inversely proportional to the spatial frequency, the increase of the values of TC results in decrease of the size of polarization speckles [39]. It is important to note that finite size of the optical system can limit the observable speckle size and may introduce diffraction effects that can alter the expected scaling behavior. Similarly, at larger scattering angles, higher-order scattering events can modify the speckle statistics, thereby, disrupting the TC scaling behavior.

We measured the polarization speckle size (PSS) by computing the spatial autocorrelation function of speckle patterns generated from non-separable vector vortex beams with topological charges $l = 1$ to 5 in 0.5 increments, after projecting the output onto a horizontally polarized state using a linear polarizer. The division factor (DF) of the polarized speckle size for two consecutive topological charges is nearly equal to $\mathrm{DF} = \frac{\mathrm{PSS}(l)}{\mathrm{PSS}(l')} \sim 1.15\mu m$. The division factor $\mathrm{DF} \sim 1.15\mu m$ is a constant which is determined by the experimental conditions such as the beam size and the propagation distance etc. It is clear from the Fig. 4(a) that the size of the speckles decreases exponentially with increasing the topological charge of the vortex beam. From the Fig. 4(a), we obtained the general expression for finding the polarization speckle size:

$$\mathrm{PSS}(l) = A\exp(-l/\delta), \tag{6}$$

where A is a constant which depends on the beam parameters determined by the experimental setup and l is an arbitrary topological charge of the vortex beam including fractional values, and δ is the decay factor. From the fitting, we obtained $A = 645.45$ μm and $\delta = 3.41$. While Eq. (6) is an empirical fit derived from the experimental data, it reflects the underlying theoretical behavior described by classical speckle theory, where the speckle size is inversely proportional to the effective aperture or angular spread of the illuminating beam. To account for the dependence of the aperture on the topological charge, the effective aperture of the beam can be modelled as $D(l) = D_0 \times \exp(kl)$, where D_0 and k are fitting parameters. Specifically, the polarization speckle size PSS(l) is given by [25]

$$PSS(l) = \frac{\lambda z}{D(l)} = \frac{\lambda z}{D_0}\exp(-kl), \tag{7}$$

where λ is the wavelength, z is the propagation distance. By comparing Eqs. (6) and (7), we obtain the relations $A = \frac{\lambda z}{D_0}$ and $\delta = \frac{1}{k}$. These results imply that the topological charge of the vector vortex beam can be obtained from the polarization speckles size of the auto-correlation function. Unlike conventional methods such as interferometry, diffraction or mode decomposition typically applied to scalar vortex beams, our technique offers a simple, non-interferometric approach based on polarization speckle analysis, presenting a novel method for estimating the topological charge of vector vortex beams.

Further, we also calculate the variation of the speckle size corresponding to the six different polarization states H, V, D, AD, RCR, LCR at a particular propagation distance (z) and order of vector vortex beams. Fig. 4(b) shows the variation of the speckle size with different polarization states $l = 2$ and $z = 20$ cm. It is clear from the Fig. 4(b) that the average speckle size is constant (blue dots) for different polarization states but there is small drift (red squares). This may be due to the change in the beam size.

We further calculate the polarization speckle size of auto-correlation function for different topological charges $l = 1$–5 for propagation distances z = 20 – 40 cm with an interval of 5 cm. We observe that the polarization speckle size varies linearly with the propagation distance for all topological charges from $l = 1$–5. The Statistical error was measured by eight data points for each polarization speckle size using eight different line profiles of the beam, for eight different images, for each order. The variation of the polarization speckle size with the propagation distance for the topological charges $l = 1$ and 3 along with the statistical error, are shown in Fig. 5. For all the orders, the error is nominal. This is due to the fact that the auto-correlation function is independent of the alignment.

We now define the divergence as the rate of change of the polarization speckle size with the propagation distance [39] i.e., the slope of the line that we obtain by using a linear fit to the data. Fig. 6(a) shows

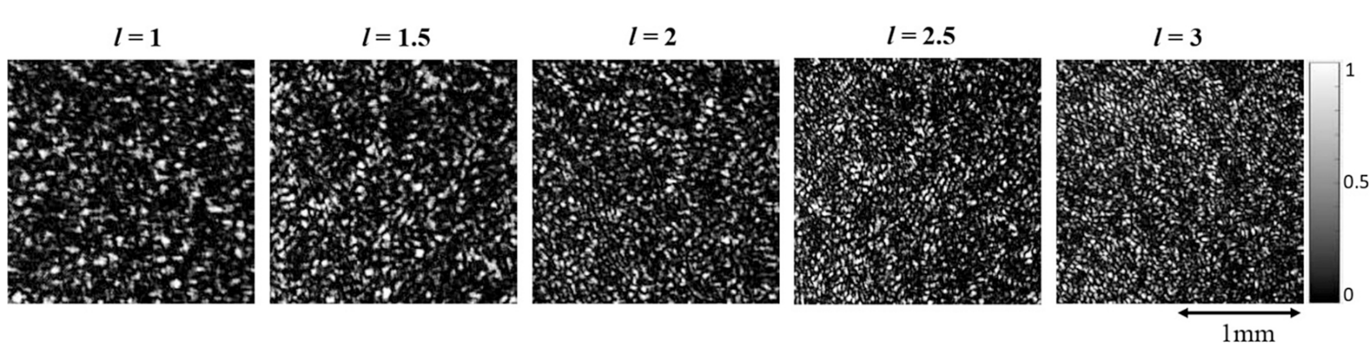

Fig. 3. The experimental images for the intensity distributions of the speckle patterns for orders $l = 1$–3 with an interval of 0.5 from left to right.

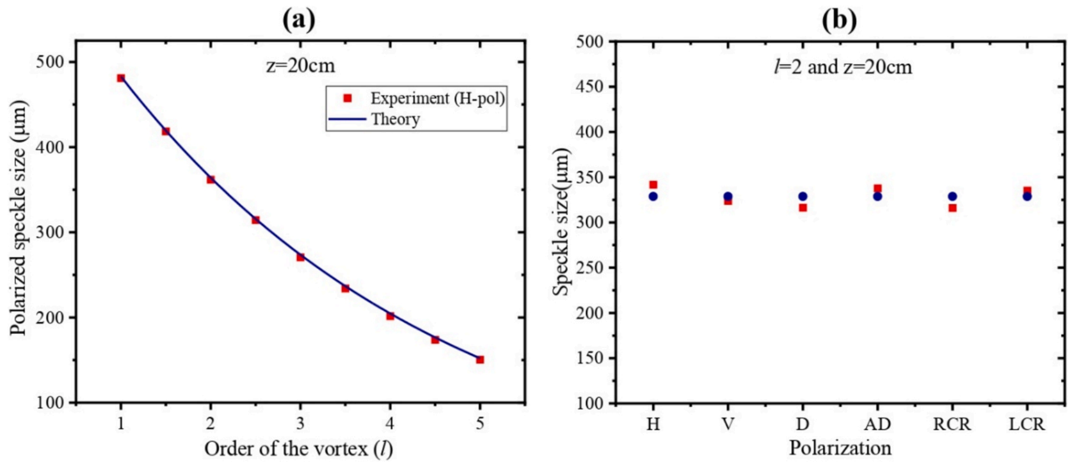

Fig. 4. Variation of the polarized speckle size with (a) the order of vector vortex beam for propagation distance z = 20 cm, (b) the different polarization projections H, V, D, AD, RCR, LCR with $l = 2$ and $z = 20$ cm.

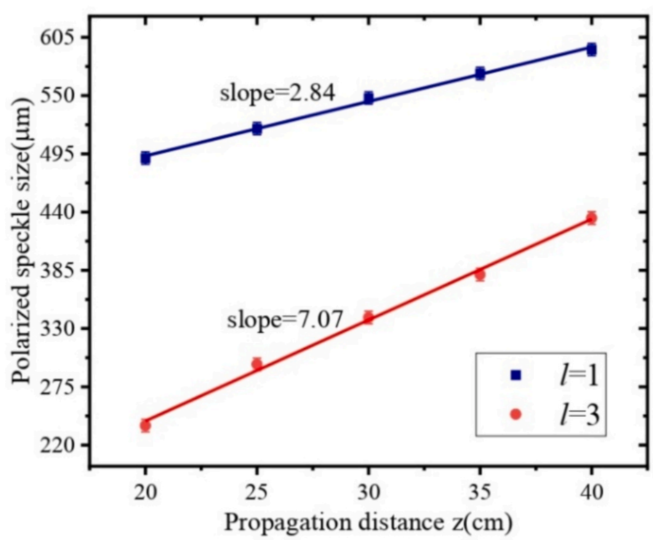

Fig. 5. Variation of polarized speckle size with propagation distance (z) for different orders $l = 1$ (blue), and $l = 3$ (red).

change in the divergence of the polarization speckles as a function of the order $l = 1 - 5$ of scattered vector vortices. It is clear from the figure that the divergence varies linearly with the order. We also define the level of accuracy for measuring the topological charge of spatial mode using experimental and theoretical divergence values as $\alpha = 1 - \frac{div_{exp} - div_{th}}{div_{exp}}$. Fig. 6(b) shows the accuracy of finding the topological charge of the vector vortex beam with not only integer but also fractional number (half integer). Therefore, the accuracy of finding the spatial mode information of the scattered vector vortex beams is more than 95 %. Therefore, in optical communication, vector vortex beams (having the high degrees of freedom) can be used to significantly improve the communication capacity.

Conclusions

We have produced the light beam with non-separable state of polarization and orbital angular momentum and generated the auto-correlation functions using the speckle patterns obtained by the scattering of vector vortex beams. We also find the polarization speckle size which is decreasing with increasing the order of the vortex beam. The experimental determination of topological charge of the vector vortex beam using its polarization speckle size of 2D spatial auto-correlation function is shown. We have also studied their propagation and used the polarization speckle size to define the divergence and found that it

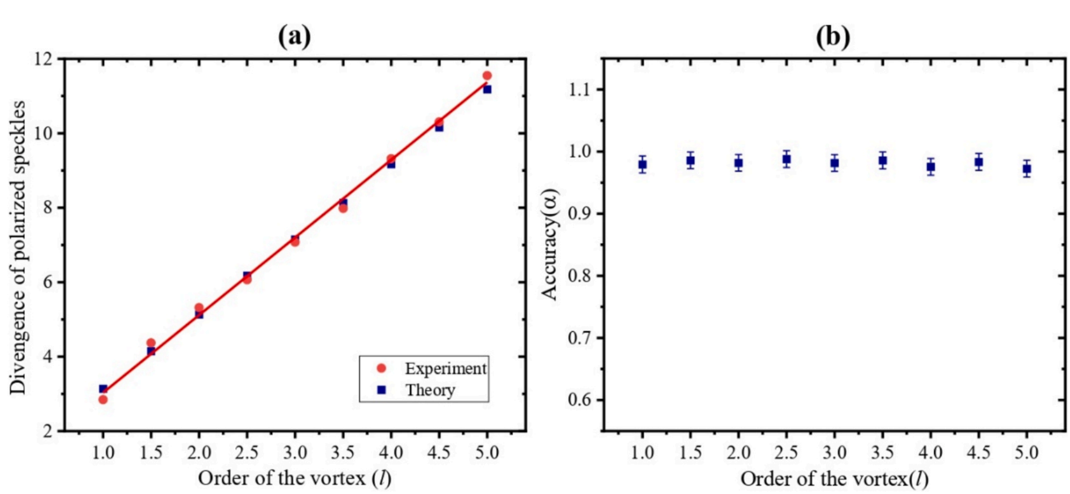

Fig. 6. (a) Experimental (red) and theoretical (blue) variation of the divergence of polarization speckles as a function of the order of scattered vector vortices, (b) The accuracy level of finding the topological charge using the divergence of the polarization speckle size.

varies linearly with propagation distance and the divergence varies linearly with the both integer and half integer orders. One may use these results to generate a 1-D key from a 2D correlation image, which will enhance the security over the key generated with just speckles patterns [40].

CRediT authorship contribution statement

Patnala Vanitha: Writing – original draft, Visualization, Software, Investigation, Formal analysis, Data curation, Conceptualization. **Do-Kyeong Ko:** Writing – review & editing, Validation, Supervision, Project administration, Methodology, Funding acquisition, Data curation, Conceptualization.

Funding

This work was supported by the National Research Foundation of Korea (NRF) grant funded by the Korea government (MSIT) (No. NRF-2021R1A2C2093138) and the AI-based GIST Research Scientist Project grant and Future-leading Specialized Research Project funded by the GIST in 2025.

Declaration of competing interest

The authors declare that they have no known competing financial interests or personal relationships that could have appeared to influence the work reported in this paper.

Acknowledgements

Authors sincerely thank to Dr. Youngbin Na for checking the theory.

Data availability

Data will be made available on request.

References

[1] Erhard M, Krenn M, Zeilinger A. Advances in high-dimensional quantum entanglement. Nat Rev Phys 2020;2:365–81. https://doi.org/10.1038/s42254-020-0193-5.

[2] Jabir MV, Apurv Chaitanya N, Mathew M, Samanta GK. Direct transfer of classical non-separable states into hybrid entangled two photon states. Sci Rep 2017;7:7331. https://doi.org/10.1038/s41598-017-07318-1.

[3] Jeong H, Zavatta A, Kang M, Lee SW, Costanzo LS, Grandi S, et al. Generation of hybrid entanglement of light. Nat Photon 2014;8:564–9. https://doi.org/10.1038/nphoton.2014.136.

[4] Liu J, Chen X, He Y, Lu L, Ye H, Chai G, et al. Generation of arbitrary cylindrical vector vortex beams with cross-polarized modulation. Results Phys 2020;19:103455. https://doi.org/10.1016/j.rinp.2020.103455.

[5] Borges CVS, Hor-Meyll M, Huguenin JAO, Khoury AZ. Bell-like inequality for the spin–orbit separability of a laser beam. Phys Rev A 2010;82:33833. https://doi.org/10.1103/PhysRevA.82.033833.

[6] Zhu Z, Janasik M, Fyffe A, Hay D, Zhou Y, Kantor B, et al. Compensation-free high-dimensional free-space optical communication using turbulence-resilient vector beams. Nat Commun 2021;12:1666. https://doi.org/10.1038/s41467-021-21793-1.

[7] Johansen SB, Töppel F, Stiller B, Banzer P, Ornigotti M, Giacobino E, et al. Classically entangled optical beams for high-speed kinematic sensing. Optica 2015;2:864. https://doi.org/10.1364/OPTICA.2.000864.

[8] Töppel F, Aiello A, Marquardt C, Giacobino E, Leuchs G. Classical entanglement in polarization metrology. New J Phys 2014;16:073019. https://doi.org/10.1088/1367-2630/16/7/073019.

[9] Aiello A, Töppel F, Marquardt C, Giacobino E, Leuchs G. Quantum-like nonseparable structures in optical beams. New J Phys 2015;17:043024. https://doi.org/10.1088/1367-2630/17/4/043024.

[10] Ndagano B, Perez-Garcia B, Roux FS, McLaren M, Rosales-Guzman C, Zhang Y, et al. Characterizing quantum channels with non-separable states of classical light. Nat Phys 2017;13:397–402. https://doi.org/10.1038/nphys4003.

[11] Allen L, Beijersbergen MW, Spreeuw RJC, Woerdman JP. Orbital angular momentum of light and the transformation of Laguerre-Gaussian laser modes. Phys Rev A 1992;45:8185–90. https://doi.org/10.1103/PhysRevA.45.8185.

[12] Mishra S, Anwar A, Singh RP. Generating arbitrary non-separable states with polarization and orbital angular momentum of light. Opt Commun 2024;554:130223. https://doi.org/10.1016/j.optcom.2023.130223.

[13] Pohl D. Operation of a Ruby laser in the purely transverse electric mode TE_{01}. Appl Phys Lett 1972;20:266–7. https://doi.org/10.1063/1.1654142.

[14] Jones PH, Rashid M, Makita M, Maragò OM. Sagnac interferometer method for synthesis of fractional polarization vortices. Opt Lett 2009;34:2560–2. https://doi.org/10.1364/OL.34.002560.

[15] Zhao B, Hu XB, Rodríguez-Fajardo V, Forbes A, Gao W, Zhu ZH, et al. Determining the non-separability of vector modes with digital micromirror devices. Appl Phys Lett 2020;116:091101. https://doi.org/10.1063/1.5142163.

[16] Marrucci L, Manzo C, Paparo D. Optical spin-to-orbital angular momentum conversion in inhomogeneous anisotropic media. Phys Rev Lett 2006;96:163905. https://doi.org/10.1103/PhysRevLett.96.163905.

[17] Chen M, Forbes A, Rosales-Guzman C. Scattering of vector vortex beams: dependence on beam parameters and medium properties. J Opt 2018;20:115603. https://doi.org/10.1016/j.rinp.2023.106588.

[18] Lei Q, Tu S, Gong H, Zhao L, Ren Y, Cai Y, et al. Construction of vector vortex beams on hybrid-order Poincaré sphere through highly scattering media. Opt Exp 2024;32:21506–16. https://doi.org/10.1364/OE.525411.

[19] Singh RK, Naik DN, Itou H, Miyamoto Y, Takeda M. Characterization of spatial polarization fluctuations in scattered field. J Opt 2014;16:105010. https://doi.org/10.1088/2040-8978/16/10/105010.

[20] Goodman JW. Speckle phenomena in optics: theory and applications. Roberts & Company 2007. https://doi.org/10.1117/3.2548484.

[21] Liu Y, Cui G, Shi S, Liao F, Cui W, Zhao J. Improving the performance of speckle correlation imaging by using a speckle refinement method with self-calibrated homomorphic filtering. Opt Laser Technol 2024;179:111328. https://doi.org/10.1016/j.optlastec.2024.111328.

[22] Zhao J, Winetraub Y, Yuan E, Chan WH, Aasi SZ, Sarin KY, et al. Angular compounding for speckle reduction in optical coherence tomography using geometric image registration algorithm and digital focusing. Sci Rep 2020;10:1893. https://doi.org/10.1038/s41598-020-58454-0.

[23] Lohmann AW, Weigelt G, Wirnitzer B. Speckle masking in astronomy: triple correlation theory and applications. Appl Opt 1983;22:4028–37. https://doi.org/10.1364/AO.22.004028.

[24] Reddy SG, Prabhakar S, Kumar A, Banerji J, Singh RP. Higher order optical vortices and formation of speckles. Opt Lett 2014;39:4364–7. https://doi.org/10.1364/OL.39.004364.

[25] Goodman JW. Statistical Optics. 2nd ed. Hoboken, NJ: Wiley; 2015.

[26] Tchvialeva L, Dhadwal G, Lui H, Kalia S, Zeng H, McLean DI, et al. Polarization speckle imaging as a potential technique for in vivo skin cancer detection. J Biomed Opt 2012;18. https://doi.org/10.1117/1.JBO.18.6.061211.

[27] Shirai T, Dogariu A. Polarization speckle dynamics in tissue-like scattering media. J Biomed Opt 2016;21:056012. https://doi.org/10.1117/1.JBO.21.5.056012.

[28] Alfano RR, editor. Biomedical Photonics: Optical Spectroscopy and Imaging. CRC Press; 2010.

[29] Chang Y, Gao W. Directly obtaining the polarization properties from measured Mueller matrices. Opt Lasers Eng 2021;139:106472. https://doi.org/10.1016/j.optlaseng.2020.106472.

[30] Huang HC, Lin YT, Shih MF. Measuring the fractional orbital angular momentum of a vortex light beam by cascaded Mach-Zehnder interferometers. Opt Commun 2012;285:383–8. https://doi.org/10.1016/j.optcom.2011.09.063.

[31] Zhu J, Zhang P, Fu D, Chen D, Liu R, Zhou Y, et al. Probing the fractional topological charge of a vortex light beam by using dynamic angular double slits. Photonics Res 2016;4:187–90. https://doi.org/10.1364/OL.40.000788.

[32] Shikder A, Nishchal NK. Measurement of the fractional topological charge of an optical vortex beam through interference fringe dislocation. Appl Opt 2023;62:D58–67. https://doi.org/10.1364/AO.476455.

[33] Alves CR, Jesus-Silva AJ, Fonseca EJS. Characterizing coherence vortices through geometry. Opt Lett 2015;40:2747–50. https://doi.org/10.1364/OL.40.002747.

[34] Vanitha P, Lal N, Rani A, Das BK, Reddy SG, Singh RP. Correlations in scattered perfect optical vortices. J Opt 2021;23:095601. https://doi.org/10.1088/2040-8986/ac094f.

[35] Vanitha P, Bhargavi M, Reddy SG, Annapuraddy V, Prabhakar S, Banerji J, et al. Intensity correlations in perturbed optical vortices: diagnosis of the topological charge. Waves Random Complex Media 2023:1–13. https://doi.org/10.1080/17455030.2023.2237132.

[36] Vanitha P, Vinny Cris M, Reddy SG, Alves CR. Correlation between coherent and scattered optical vortices: diagnosis of the topological charge. Appl Phys B 129 2023:85. https://doi.org/10.1007/s00340-023-08027-6.

[37] Vanitha P, Na Y, Kyeong Ko D. Characterizing the fractional coherence vortices through the area of the intensity cross-correlation function. J Opt Soc Am A 2024;41:1397–402. https://doi.org/10.1364/JOSAA.527925.

[38] Perumangatt C, Reddy SG, Anwar A, Aadhi A, Prabhakar S, Singh RP. Scattering of non-separable states of light. Opt Commun 2015;355:301–5. https://doi.org/10.1016/j.optcom.2015.06.066.

[39] Reddy SG, Permangatt C, Prabhakar S, Anwar A, Banerji J, Singh RP. Divergence of optical vortex beams. Appl Opt 2015;54:6690–3. https://doi.org/10.1364/AO.54.006690.

[40] Vanitha P, Manupati B, Muniraj I, Anamalamudi S, Reddy SG, Singh RP. Augmenting data security: physical unclonable functions for linear canonical transform-based cryptography. Appl Phys B 2022;128:183. https://doi.org/10.1007/s00340-022-07901-z.